

## NUMERICAL INVESTIGATION OF RC TUNNEL SEGMENTS SUBJECTED TO ELEVATED TEMPERATURE VIA FEM

Tolga YILMAZ<sup>1\*</sup>, Uğurhan AKYÜZ<sup>2</sup>

<sup>1</sup> Konya Technical University, Faculty of Engineering and Natural Sciences, Department of Civil Engineering, Konya, Turkey, ORCID No : <http://orcid.org/0000-0001-7668-1496>

<sup>2</sup> Middle East Technical University, Faculty of Engineering, Department of Civil Engineering, Ankara, Turkey, ORCID No : <http://orcid.org/0000-0003-1210-8142>

### Keywords

Tunnel segments  
Finite element method  
Numerical analysis  
Elevated temperature

### Abstract

There has been increasing concern about the fire-resistant design of reinforced concrete tunnel lines among structural engineers due to the fire incidents that occurred recently. A limited number of experimental works focused on the fire behavior of the conventional reinforced concrete (RC) and hybrid fiber reinforced concrete (HFRC) tunnel segments have been presented in the literature. However, there is no comprehensive numerical study related to RC shield tunnel segments under the effect of elevated temperature. Thus, this study intends to establish a 3D finite element model (FEM) for the evaluation of the fire behavior of RC shield tunnel segments. At the first stage of the presented FEM, the temperature distribution that occurred in the RC tunnel segment was evaluated with a heat transfer analysis carried out. In the second stage, the stress analysis was conducted to calculate the load-displacement behavior of the RC tunnel segment under the combined effect of the gravity load and the elevated temperature. The results obtained from the FEM were compared with an experimental work existing in the literature. The fact that numerical analysis is compatible with experimental results proves that the presented FEM can be used in the determination of the behavior of RC shield tunnel segments subjected to elevated temperature.

## ARTAN SICAKLIK ETKİSİNDEKİ BETONARME TÜNEL SEGMANLARININ SEM İLE SAYISAL OLARAK İNCELENMESİ

### Anahtar Kelimeler

Tünel segmanları  
Sonlu elemanlar yöntemi  
Nümerik analiz  
Sıcaklık artışı

### Öz

Son zamanlarda meydana gelen yangın olayları nedeniyle yapı mühendisleri arasında betonarme tünel hatlarının yangına dayanıklı tasarımına ilgi giderek artmaktadır. Literatürde geleneksel betonarme (RC) ve hibrit fiber donatılı beton (HFRC) tünel segmanlarının yangın davranışına odaklanan sınırlı sayıda deneysel çalışma sunulmuştur. Ancak, yüksek sıcaklık etkisindeki RC kalkan tünel segmanları ile ilgili kapsamlı bir sayısal çalışma bulunmamaktadır. Bu nedenle, bu çalışma, RC kalkan tünel segmanlarının yangın davranışının değerlendirilmesi için bir 3B sonlu eleman modeli (SEM) oluşturmayı amaçlamaktadır. Sunulan SEM'in ilk aşamasında, RC tünel segmentinde meydana gelen sıcaklık dağılımı, gerçekleştirilen ısı transferi analizi ile değerlendirilmiştir. İkinci aşamada, düşey yük ve artan sıcaklığın birleşik etkisi altında RC tünel segmentinin yük-deplasman davranışını hesaplamak için gerilme analizi yapılmıştır. SEM'den elde edilen sonuçlar literatürde yer alan deneysel bir çalışma ile karşılaştırılmıştır. Sayısal analizin deneysel sonuçlarla uyumlu olması, sunulan FEM'in yüksek sıcaklığa maruz RC kalkan tünel segmanlarının davranışının belirlenmesi için kullanılabileceğini göstermiştir.

Araştırma Makalesi

Başvuru Tarihi

Kabul Tarihi

: 18.04.2022

: 07.06.2022

Research Article

Submission Date

Accepted Date

: 18.04.2022

: 07.06.2022

\* Corresponding author; e-mail : tyilmaz@ktun.edu.tr



Bu eser, Creative Commons Attribution License (<http://creativecommons.org/licenses/by/4.0/>) hükümlerine göre açık erişimli bir makaledir.

This is an open access article under the terms of the Creative Commons Attribution License (<http://creativecommons.org/licenses/by/4.0/>).

## 1. Introduction

The fire-resistant design of the tunnel lines has gained importance due to several significant tunnel fire incidents which occurred worldwide including the Great Belt Tunnel (Denmark, 1994), the Channel Tunnel (England–France, 1996), the Mount Blanc Tunnel (France–Italy, 1999), and the St. Gothard Tunnel (Switzerland, 2001). The major tunnel fire incidents caused injuries to people, non-functionalized facilities, and damage to the concrete lining, by affecting negatively structural adequacy in the past. It should be considered that there is also a significant economic impact since the tunnel becomes close during the restoration works (Guerrieri, Sanabria, Lee, Pazmino and Patel, 2020). The maximum temperature, quick heating rate, long duration, and temperature gradient with non-uniform are characteristics of the tunnel fire. Therefore, tunnel linings may experience severe damage and complex failures with the effect of the tunnel fire. In addition to the deterioration observed in the strength properties of concrete due to the high temperature, severe concrete spalling is also a major issue to be considered for the safety of the concrete tunnel lines in case of tunnel fires. Besides, for a metro shield tunnel lining constructed Tunnel Boring Machine (TBM) technique, the configuration and joint connections of the shield lining segments may lead to further complexities (Yan, Shen, Zhu, Li and Lu, 2015).

The recommendations and requirements that are related to tunnel linings' fire safety have existed in some guidelines and specifications (International Tunnelling and Underground Space Association (ITA), Guidelines for structural fire resistance for road tunnels, 2005; European Committee for Standardization (CEN) Eurocode 1: actions on structures, EN 1991-1-2, 2002; National Fire Protection Association (NFPA), NFPA 502 standard for road tunnels, bridges, and other limited-access highways, NFPA 502, 1998). The issues such as the damage to tunnel lining due to fire, the measurement of fire protection, and the rehabilitation process of damaged tunnel lining have been studied and documented in The European EUREKA program and The European UPTUN project (NFPA 502, 1998; Haack, 1992; Haack, 1998; Lönnermark, 2005). For unload state, the isolated K segment belonging to a TBM tunnel has been investigated by Caner and Böncü (2009) with the hydrocarbon fire experiments conducted. It is found that under the effect of the hydrocarbon fire, the safety factor deviation of the TBM tunnel increased from soft soil to stiff soil conditions while the tunnel exhibited more flexible behavior. Yasuda and Ono (2004) carried out an experimental program to investigate the measurement of the fire protection for composite TBM tunnel segments subjected to a RABT fire curve. Test results unveiled that when the fire protection is not

applied on the surface, the concrete spalling attained up to 60 mm. In the experimental work of Yan, Zhu, Ju and Ding (2012), the fire behavior of the full-scale reinforced concrete (RC) TBM tunnel linings have been examined. Based on the ISO834 protocol, heating durations of 45 90 minutes were applied to the RC TBM tunnel linings. At the end of the experiments, it is found that severe concrete explosive spalling and the decrease in the elastic modulus and strength belonging to the joint bolt occur with the effect of high temperatures. Therefore, it is determined that the tunnel lining joints' flexural stiffness considerably decreased. The coupled thermo-mechanical actions led to a significant increase in the opening angles and the gaps, which exist in the tunnel lining joints. Furthermore, it is concluded that the temperature of the reinforcement on the heated side could go beyond the failure temperature under the ISO834 fire test with a duration of 90 minutes. Hua, Khorasani, Tessari and Ranade (2022) investigated experimentally the effects of concrete composition, polypropylene fiber additions, the structural constraint level, and fire characteristics on the fire performance of RC tunnel slabs. There are limited numbers of works where the full-scale tunnel linings are tested under the combined effects of the structural load and fire by considering the actual boundary conditions and the conditioning which correspond to design assumptions (Guerrieri et al., 2020; Siemon and J. Zehfuß, 2017; Richter, 2005; Kaundinya, Dehn, Nause and Juknat, 2009; Boxheimer, Knitl and Dehn, 2009). Alhawat, Hamid, Baharom, Azmi, and Kaish (2021) studied the fire performance of the unloaded tunnel rings with different mixed designs through extensive full-scale tests. Numerical studies related to the behavior of RC structural elements exposed the fire have been also presented in the literature (Gao, Dai, Teng and Chen, 2013; Hajiloo and Green, 2018; Pagani, Bocciarelli, Carvelli and Pisani (2014); Dai, Gao and Teng, 2015). Jiang, Orabi, Jiang and Usmani (2021) developed a novel FEM code where a thermo-mechanical nonlinear shell element and a plane-stress formulation of the concrete damage-plasticity material were utilized. Shen, Zhu, Yan, Zhou and Lu (2021) introduced a semi-analytical thermo-mechanical model for segmental joints exposed to fire. To assess the heating and cooling behavior of the RC tunnel slabs, the FEM model has been developed by Hua, Khorasani, and Tessari (2022).

The main motivation of the present study is to develop a novel 3D finite element model (FEM) that can be utilized for the evaluation of the RC shield tunnel segments subjected to the combined effect of mechanical loading and elevated temperature. The proposed FEM was verified by a previous experimental study presented by Yan et al. (2015). With the comparison of numerical and test results, it has been deduced that the developed FEM

can be safely used for the evaluation of the temperature distribution and the load-deflection behavior of the mechanically loaded RC shield tunnel segments subjected to fire.

**2. Overview of Experimental Study Used for the Verification of the FE model**

The verification of the present FEM has been carried out using the results obtained from the study presented by Yan et al. (2015). This study has provided useful experimental data related to the thermo-mechanical performance of both RC and hybrid reinforced concrete (HFRC) shield TBM tunnel segments with consideration of various boundary and loading conditions. In the scope of the test program, the test specimens have been designed and manufactured at a scale factor of 1/3 concerning the full-size lining units. The width, thickness, and average radius of the test specimens are 300 mm, 120 mm, and 990 mm, respectively. Besides, the details existing in the real metro TBM tunnel line like hand holes, circumferential tongues, and grooves were also manufactured in the test specimens. The concrete cover thickness was 15 mm. The geometrical dimensions and reinforcement details were given in Figure 1 (Yan et al., 2015).

The concrete compressive strength of the standard cubic samples measured on the 28th day under the ambient temperature conditions was 69.8 MPa. The elastic modulus and the tensile strength of first-grade steel reinforcement are 206 GPa and 300 MPa, respectively. A gas temperature is a unit of °C. The experimental program has been carried out using the test setup which enables testing tunnel lining segments under the effect of various combinations of static loading and elevated temperatures. The test setup is composed of a furnace with two combustors that are industrial-grade and a mechanical loading frame. The specific heating-up history can be defined through a programmable system controlling the furnace. In the experimental program, the Eurocode HC curve (Eurocode 1, 2002) was used for modeling the heating phase and it can be expressed as follows: (Gao et al., 2013):

$$T = 20 + 1080(1 - 0.325e^{-0.167t} - 0.675e^{-2.5t}) \tag{1}$$

where t shows time in units of minutes, and T refers to the furnace gas temperature in °C. The overall test setup and the insulated tunnel segment placed above the furnace were depicted in Figure 2 (Yan et al., 2015). Two insulation panels were placed on the two opposite sides of the RC tunnel segment, and also the ceramic fibers filled the gaps between specimen and panels to achieve one face heating uniformly.

In the conducted test program, the external pressure load exerted by surrounding soil has been represented with two-point loads acting on one-third of the RC tunnel segment span. Besides, since a segment constituting a tunnel shield ring may be exposed to positive or negative moments in the service period depending on its location, these effects have been considered in the experimental program by applying the horizontal loads to two ends of the RC tunnel segment through the horizontal activators. Therefore, in the experimental program, three different boundary conditions such as the free sliding, the no sliding, and the case aiming to generate a negative moment occurring at the central section of the RC segment have been generated by applying no horizontal load or the controlled horizontal loads.

Furthermore, in the scope of the experimental program, four different patterns of mechanical and fire loading, which are named ambient temperature, post-fire, under-fire, and heating to failure, have been considered. In the ambient temperature test, the RC tunnel segment is tested under the vertical load without a fire effect. The post-fire test has focused on the residual strength of the RC tunnel segment after its exposure to fire. In this combination, the RC tunnel segment loaded up to its service load level was subjected to a heating and cooling

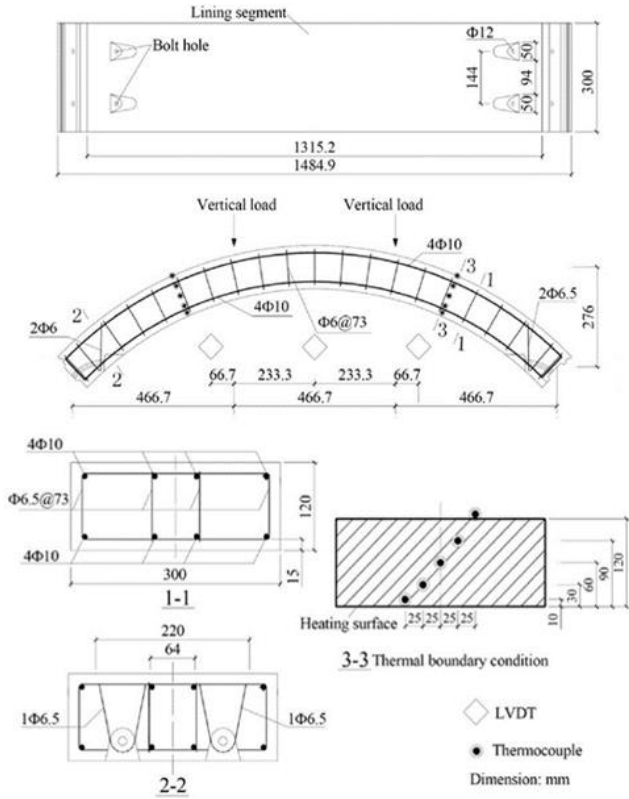


Figure 1. The geometrical dimensions and rebar details of the RC tunnel segment (Yan et al., 2015)

cycle considering the Eurocode HC curve, and then the RC tunnel segment was tested under the effect of the vertical mechanical load until the failure to specify the ultimate strength of the RC tunnel segment after the fire. In the under-fire test, the RC tunnel segment without any initial mechanical load was subjected to the heating for 40 minutes, and then it was statically loaded to examine the ultimate strength.

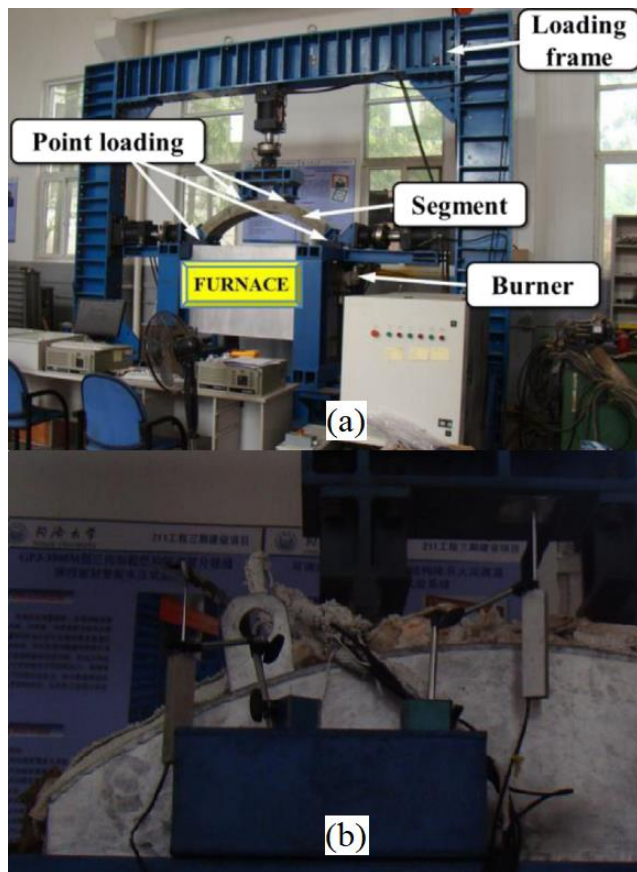


Figure 2. (a) The overall test setup (b) the insulated tunnel segment placed the above the furnace (Yan et al., 2015)

In the heating to failure test, which was used for verification of the numerical model, first, the RC tunnel segment was mechanically loaded up to 80% of its ultimate load level. Then the RC tunnel segment was exposed to heating that follows the Eurocode HC curve and held at the maximum temperature level until the failure of the test specimen under the combined effect of the mechanical loading and elevated temperature. The initial static load and the heating time were approximately 60 kN and 42 min for the RC tunnel segment test specimen with free-sliding boundary condition, which had been used for verification and named RC3 in the experimental study (Yan et al., 2015). The temperature gradient, midspan deflection, the vertical and lateral forces were measured during the

experiments. Temperature measurements have been taken from two different cross-sections depicted in Figure 1 using K-type thermocouples. Besides, a non-contact, high-sensitivity infrared radiometer was utilized to verify the accuracy of the temperature measurements.

### 3. Finite Element Modeling Procedure

In the scope of the study, the numerical analysis has been conducted using ABAQUS software. The Standart Module of ABAQUS utilizes the Newton-Raphson algorithm for the solution of nonlinear problems. The finite element model (FE model) developed has been based on a sequential thermal-stress analysis (STSA) technique. Heat transfer analysis (HTA) is the first step of STSA. Then, stress analysis (SA) is carried out by importing the nodal temperatures calculated from the HTA stage. The SA considers the combined effect of the static load and the elevated temperature. The presented finite element procedure has included another stage for the static load before the fire analysis. Therefore, the FE model developed consists of three different stages which are the HTA, the SA considering only static load, and the SA performed under the combined effect of static load and elevated temperature.

In the first step of the FE model, the geometries of concrete and steel rebar were modeled as discrete in the part module of ABAQUS. The STSA requires that two FE models with identical configurations are generated. While one of them was used in the HTA, the other was for the SA including the elevated temperature effect. The number of elements generated in the model and the mesh arrangement of the parts that composed both two assemblies must be identical so that the nodal temperature data can be transferred to the stress analysis. In the second step, the thermal and mechanical properties belonging to the concrete and steel reinforcements were defined. After the second step, the element types used in the FE model, restraint conditions, and load pattern become different for heat transfer and stress analysis. The third step is heat transfer analysis. The heat transfer analysis has been carried out by using one of the standard fires which exist in codes (ASTM E119, 2015; ISO 834-1, 1999; EN1992-1-2, 2004). In the fourth step, the structural static loads were applied to the RC tunnel segment in the stress analysis model at ambient temperature. Therefore, the stress/strain states, load-deflection behavior, and crack distributions of the RC tunnel segments were obtained before the fire. In the last stage of the numerical model, the nodal temperature data calculated in the HTA stage has been transferred into the SA model, and the static loads and elevated temperature effects were calculated simultaneously at each time interval of the numerical analysis.

In the HTA of the FE model developed, the RC tunnel segment and steel loading plates were modeled with the eighth-node continuum (DC3D8), and steel rebars were modeled using the two-node link (DC1D2) thermal elements. During the SA, the FE mesh arrangement is identical to that used in the HTA, however, the thermal elements have been changed with stress elements. In the stress analysis, the eighth-node continuum with reduced integration (C3D8R) element was utilized for the modeling of the RC tunnel segment and steel loading plates while the steel rebars were modeled with the two-node link (T3D2) elements. At the end of the mesh study considering the computational time and the convergence to experimental results together, the optimum mesh sizes of the RC tunnel segment, longitudinal reinforcement, and shear reinforcement were determined as 15, 30, and 10 mm respectively. Besides, a perfect bond assumption was made for steel-to-concrete interfaces via the "embedded region" method existing in ABAQUS. In the numerical analysis, only vertical translational movement of the most bottom nodes of the RC tunnel segment, which contact with the surface of the test setup, was restrained to provide the free-sliding boundary conditions like in the test.

In the HTA, the convection, radiation, and conduction are three required heat-transfer modes to determine the temperature gradient along the RC tunnel segment. In the furnace fire, the heat fluxes flow towards the outermost surfaces of the RC tunnel segment. In this region, convection and radiation are modes of exchanging heat. However, in the concrete part, heat transfer takes place via conduction. Therefore, the temperature distribution in an RC tunnel segment can be expressed by Fourier's differential equation defined for heat conduction (Gao et al., 2013):

$$\frac{\partial}{\partial x}\left(k\frac{\partial T}{\partial x}\right) + \frac{\partial}{\partial y}\left(k\frac{\partial T}{\partial y}\right) + \frac{\partial}{\partial z}\left(k\frac{\partial T}{\partial z}\right) + Q = \rho c \frac{\partial T}{\partial t} \quad (2)$$

where  $t$  refers to time. Temperature-dependent conductivity and specific heat are  $k$  and  $c$ , respectively.  $P$  denotes density. The intrinsically generated heat  $Q$  becomes zero in HTA belonging to the RC tunnel segment. The temperature distribution at the initial and the convenient boundary conditions was used for the solution of the differential equation given in Equation 2. The temperature distribution in the RC tunnel segment at  $t=0$  is expressed as (Gao et al., 2013):

$$T(x, y, z, t)|_{t=0} = T_0(x, y, z) \quad (3)$$

where  $T_0(x, y, z)$  denotes the ambient temperature of the RC tunnel segment, of which value has been measured with thermocouples. Heat is transmitted from the fire to

the surface of the RC tunnel segment by way of convection and radiation, which can be expressed utilizing the Robin boundary conditions (Gao et al., 2013):

$$-k \frac{\partial T}{\partial n} = h_c(T - T_f) + \sigma \varepsilon_m \varepsilon_f \left[ (T - T_z)^4 - (T_f - T_z)^4 \right] \quad (4)$$

where  $n$  refers to the normal of the RC tunnel segment surface. The convective heat transfer coefficient is represented with  $h_c$  and this coefficient has been taken as 25 W/(m<sup>2</sup>K) and 9 W/(m<sup>2</sup>K) for fire exposed and unexposed surfaces, respectively (Gao et al., 2013; Hajiloo and Green, 2018).  $T_f$  is the fire temperature measured in the furnace or determined from the standard fire curve.  $T_z$  denotes the absolute zero temperature which is set at 273.15 °C. The  $\sigma$  denotes Stefan-Boltzmann constant which is equal to 5.67 x 10<sup>-8</sup> W/(m<sup>2</sup>K<sup>4</sup>). The  $\varepsilon_m$  and  $\varepsilon_f$  are the heat emissivities of the exposed surfaces and the fire, respectively. These coefficients were taken as 0.8 and 1.0 for concrete and the standard fire condition, respectively, according to Eurocode 2 (EN1992-1-2; 2004).

#### 4. Material Models

The nonlinear behavior of concrete is characterized by the Concrete damaged plasticity (CDP) model in ABAQUS. In the CDP, as consideration of compression, a linear behavior is observed up to initial yield  $\sigma_{co}$ . The stress-hardening and then strain-softening follows this threshold. The strain-softening has come after ultimate stress,  $\sigma_{cu}$ . Regarding tension, linearity is up to the failure stress  $\sigma_t0$  in which the first micro-crack is formed. After this stress, the softening stress-strain behavior occurs. The elastic stiffness degradation is described with tensile ( $d_t$ ) and compression ( $d_c$ ) damage variables, of which values vary between 0 and 1. Zero and one correspond to no damage and full loss of strength, respectively. Consequently, for tension and compression, the stress-strain relationship can be written as follows (Abaqus, 2014):

$$\sigma_t = (1 - d_t)E_0(\varepsilon_t - \bar{\varepsilon}_t^{pl}) \quad (5)$$

$$\sigma_c = (1 - d_c)E_0(\varepsilon_c - \bar{\varepsilon}_c^{pl}) \quad (6)$$

Eq. 5 and 6 can be rewritten in compact forms as follows (Li, Hao, and Bi, 2017):

$$d_t = 1 - \frac{\sigma_t/E_0}{\bar{\varepsilon}_t^{pl} \left( \frac{1}{d_t} - 1 \right) + \sigma_t/E_0} \quad (7)$$

$$d_t = 1 - \frac{\sigma_t/E_0}{\tilde{\varepsilon}_t^{pl} \left( \frac{1}{b_t} - 1 \right) + \sigma_t/E_0} \quad (8)$$

where the tensile and compressive equivalent plastic strains are  $\tilde{\varepsilon}_t^{pl} = b_t(\varepsilon_t - \frac{\sigma_t}{E_0})$  and  $\tilde{\varepsilon}_c^{pl} = b_c(\varepsilon_c - \frac{\sigma_c}{E_0})$ , respectively.  $E_0$  represents elastic modulus. A previous experimental study recommended the values of  $b_t$  and  $b_c$  as 0.2 and 0.7, respectively (Birtel and Mark, 2006). It has been demonstrated in the previous works that these values yielded accurate results for concrete materials subjected to the reversed-cyclic load and the impact load (Li, Hao, and Bi, 2017; Yılmaz, Kırac, Anil, Erdem and Sezer, 2018; Yılmaz, Kırac, Anil, Erdem and Hoşkal, 2020; Yılmaz, Kirac, Anil, Erdem and Kacaran, 2020). However, in the present study, the values of  $b_t$  and  $b_c$  has been defined as 0.2 and 0.5, respectively. The values of  $b_t$  and  $b_c$  were determined by the trial and error approach for convergence to experimental results and maintained constant for all temperature values. The dilation angle ( $\psi$ ), the flow potential eccentricity ( $e$ ), the ratio of initial equibiaxial compressive yield stress to initial uniaxial compressive yield stress ( $\sigma_{b0}/\sigma_{c0}$ ), the coefficient related to the deviatoric cross-section's shape ( $K_c$ ), and the viscosity parameter ( $\mu$ ) are other the CDP parameter that should be defined in numerical analysis. These parameters establish yield surface functions, material viscosity, and potential flow they have been defined as 30, 0.10, 1.16, 0.6667, and 0.0001, respectively, in the numerical analysis (Li et al., 2017; Yılmaz et al., 2018, 2020a, 2020b). It is assumed that they are the same for all temperatures.

The temperature-dependent uniaxial stress-strain behavior of concrete has been defined considering the approach presented in Eurocode 1992-1-2. First, it has been assumed that the initial yield stress for uniaxial behavior is  $0.33f_{c,\theta}$ . The  $f_{c,\theta}$  refers to concrete compressive strength for the considered temperature value  $\theta$ . The stress-strain path is linear up to the initial yield stress, and then the nonlinear behavior is defined with a curve expressed in Eq. 9 until the maximum compressive strength occurs. After peak stress, the softening behavior of the concrete material is described with a linear descending branch. The temperature-dependent maximum concrete compressive strength  $f_{c,\theta}$  given in Eq. 9, the strain corresponding to this peak stress  $\varepsilon_{c1,\theta}$ , also ultimate strain  $\varepsilon_{cu,\theta}$  has been defined according to the Eurocode 1992-1-2 considering temperature and aggregate type.

$$\sigma_\theta = \frac{3\varepsilon f_{c,\theta}}{\varepsilon_{c1,\theta} \left( 2 + \left( \frac{\varepsilon}{\varepsilon_{c1,\theta}} \right)^3 \right)} \quad (9)$$

The tensile strength was calculated according to the equation given in Eq. 10 (Yılmaz et al., 2018).

$$f_t = 0.623\sqrt{f_c} \quad (10)$$

While the tensile response was characterized as linear up to the peak tensile stress, the post-peak response was defined as a linear decrease. The ultimate tensile strain ( $\varepsilon_{tu}$ ) has been defined ten times of  $\varepsilon_{t1}$  which denotes tensile strain corresponding to the maximum tensile stress. This approach has been used in the previous study in the literature (Mirza and Uy, 2009). The temperature-dependent maximum tensile stress has been calculated according to the Eurocode 1992-1-2 and expressed in Eq. 11. The tensile and compression behaviors of concrete used in the numerical analysis were depicted in Figure 3 (Abaqus, 2014).

$$f_{t,\theta} = k_\theta f_t$$

$$k_\theta = 1; 20^\circ\text{C} \leq \theta \leq 100^\circ\text{C}$$

$$k_\theta = 1 - (\theta - 100)/500; 100^\circ\text{C} < \theta \leq 600^\circ\text{C} \quad (11)$$

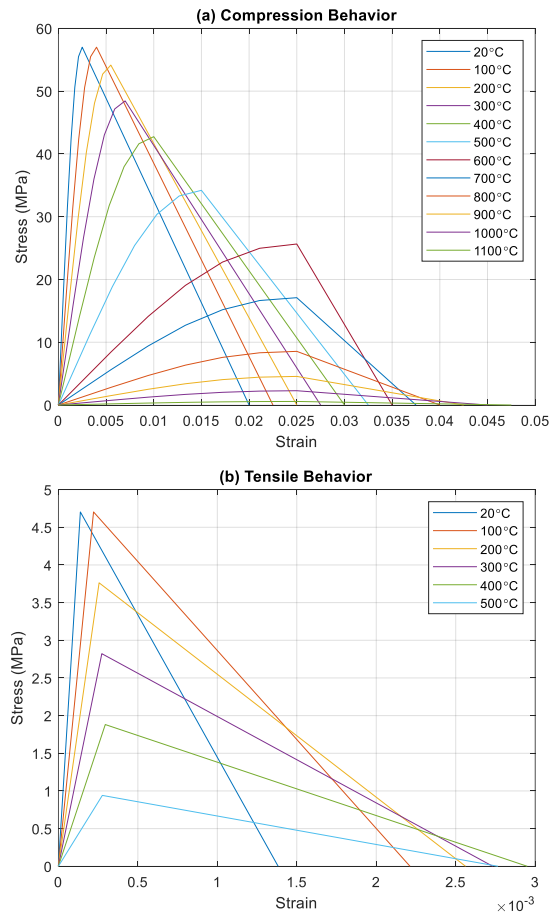


Figure 3. Compression (a) and tension (b) behaviors of concrete

It should be noted here that the minimum compressive and tensile stresses corresponding to the ultimate strains were assumed as  $0.05f_{c,\theta}$  and  $0.05f_{t,\theta}$ , respectively, instead of zero to prevent numerical instability (Gao et al., 2013; Hajiloo and Green, 2018). The concrete density was taken as  $2400 \text{ kg/m}^3$ . Poisson's ratio of concrete material was defined as 0.2. These values were kept constant at all temperatures. Specific heat of concrete and concrete conductivity was determined according to Eurocode 2 (EN1992-1-2; 2004). The specific heat and conductivity of concrete were presented in Figure 4. For thermal conductivity, Eurocode 1992-1-2 mean values were used in numerical analysis.

Steel material was modeled as elastoplastic without hardening in the numerical analysis. Specific heat and conductivity values of steel and the reductions of the steel material's elastic modulus and yield strength with the temperature increase were calculated according to Eurocode 1993-1-2 (EN1993-1-2; 2005). The specific heat and conductivity of steel were presented in Figure 5.

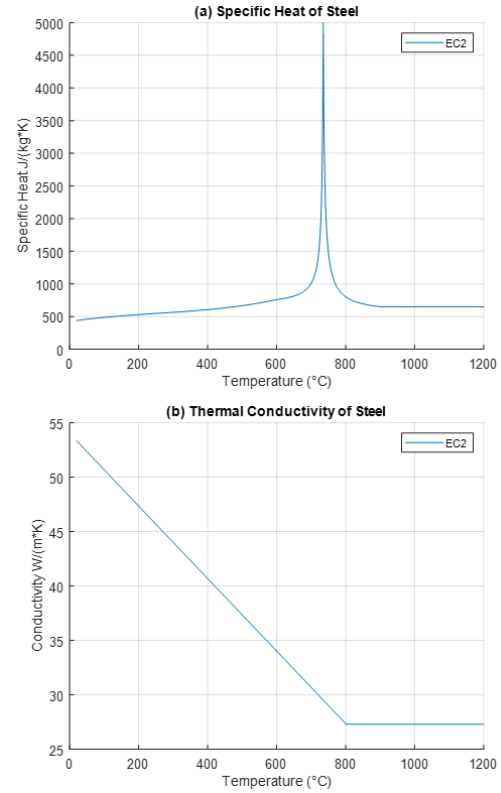


Figure 5. Specific heat (a) and thermal conductivity (b) of steel.

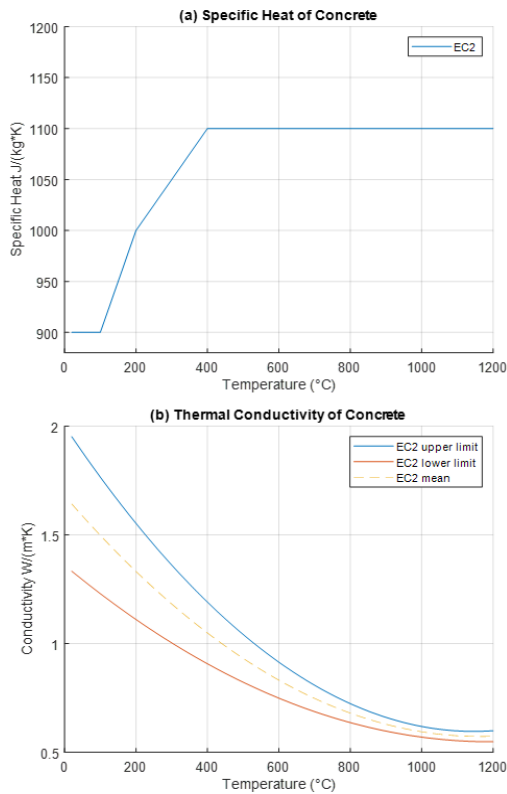


Figure 4. Specific heat (a) and thermal conductivity (b) of concrete.

### 5. Results Obtained by Numerical Analysis

The temperature distribution along the RC tunnel segment, and the load-deflection behavior under the combined effect of mechanical load and fire, crack patterns have been calculated via numerical analysis performed. Figure 6 has depicted the temperature distribution that occurred in the RC tunnel segment. Figure 7 shows the temperature time-history of the nodes obtained from numerical analysis. These nodes correspond to points where thermocouples were placed during the test. Furthermore, Figure 8 illustrates the comparison of the nodal temperatures obtained from numerical analysis and the temperature measurements in the test.

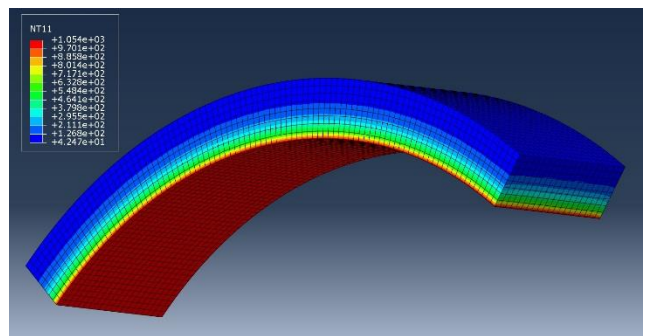


Figure 6. The temperature gradient

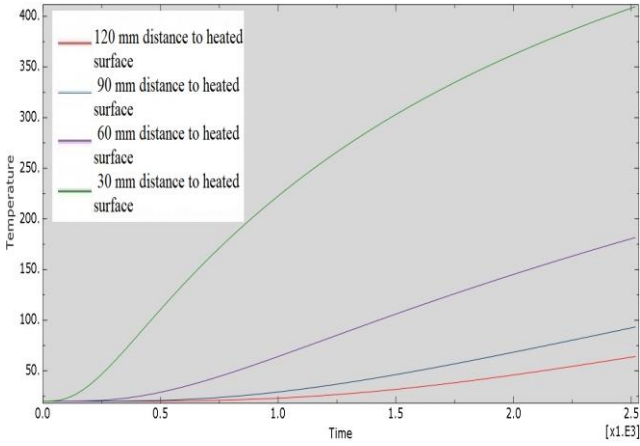


Figure 7. Temperature time-history of the nodes corresponding to points where thermocouples were placed during the test

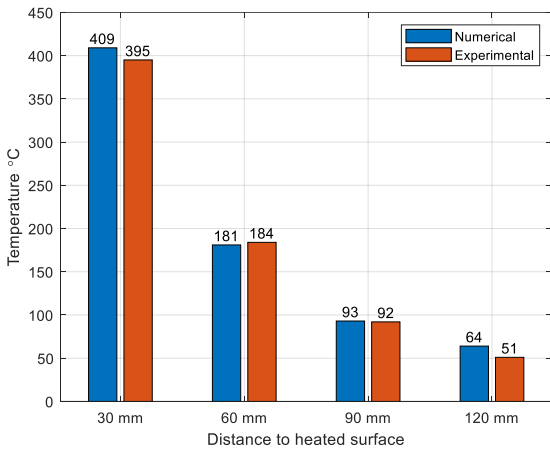


Figure 8. The comparison of the nodal temperatures obtained from numerical analysis and the temperature measurements in the test

When numerical and experimental temperature values are analyzed, it is concluded that heat-transfer analysis performed has been successful at the calculation of temperature distributions through the RC tunnel segment. The maximum, minimum, and average difference between temperature results were obtained as 20%, 1%, and %6.5, respectively. The maximum difference has occurred in the outermost of the RC tunnel cross-section. It is considered that this difference stems from the non-homogenous nature of concrete which causes variation in the conductivity of the concrete.

The damage pattern and the maximum principal stress distribution that occurred in static loading (a, c) and fire analysis (b, d) were presented in Figure 9. Damage has been characterized by values of between 0 and 1 where zero means no damage and one means total loss of

bearing capacity. Stress values are in Pa. It should be observed from Figure 9 that with the effect of the increasing temperature, widths and numbers of cracks and the principal stress also increased.

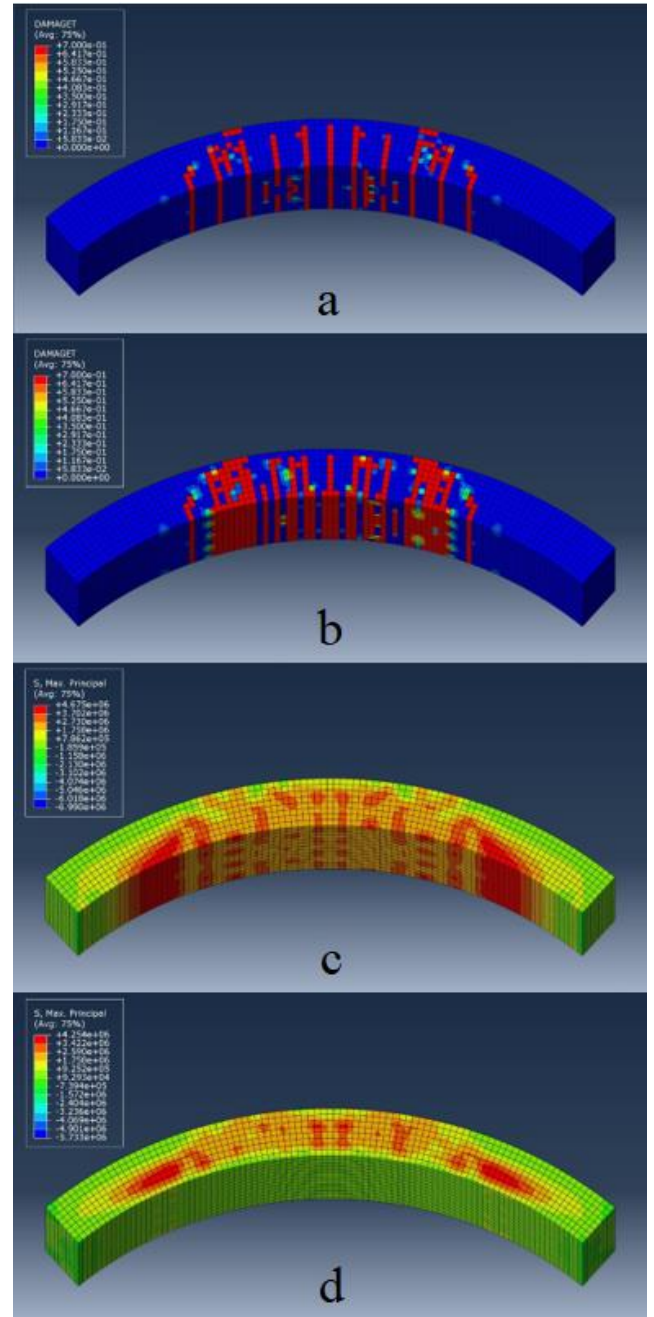


Figure 9. The damage pattern and the maximum principal stress distribution in static loading (a, c) and fire analysis (b, d)

Figure 10 shows the comparison of the load-deflection behavior obtained from numerical analysis and the test. When numerical and experimental load-deflection behaviors are examined, it is found that there is a

considerable difference between initial stiffness values, and the numerical model behaves more rigidly. It is considered that this difference results from the non-homogenous behavior of concrete. The numerical model exhibited exact homogenous material behavior in all sections. The actual test specimen has non-homogeneous nature and the damages and cracks that occurred vary the behavior. To reflect actual damage accumulation exactly in the numerical model may not be possible. Therefore, initial stiffness values were obtained differently in numerical and test results. However, the ultimate load capacity and also the displacement value at peak load, which are obtained from the numerical analysis and the experiment, are coincided and these values are 60 kN and 12.5 mm. Furthermore, ultimate displacement values are quite close in the numerical model and test, which are 49 mm and 45 mm, respectively. Consequently, the presented numerical model yields accurate results in terms of load-deflection behavior and can be used for the evaluation of the RC tunnel subjected to static load and fire effect.

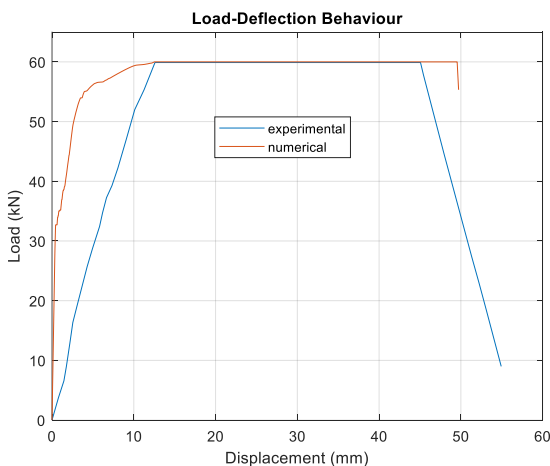


Figure 10. The numerical and experimental load-deflection behaviors

## 6. Conclusions

In the scope of this study, a 3D finite element procedure based on a sequential thermal-stress analysis technique is established for the evaluation of the fire behavior of RC shield tunnel segments. The first step of the sequential thermal-stress analysis composes of heat transfer analysis. The second step is stress analysis where the nodal temperatures obtained from the heat transfer analysis stage have been transferred, and the combined effect of the static load and the temperature increase is considered. The finite element model developed has been verified with test results taken from a comprehensive experimental study previously presented in the literature. The comparison of

numerical and experimental results reveals that the ultimate load capacity and the displacement at this peak load can be exactly calculated via the presented FEM. It is also demonstrated the ultimate displacement can be determined with a difference of 8%. Besides, it is found that the average difference for temperature distribution is only 1%. These results prove that the presented FEM can be used to predict temperature distribution occurred in the RC tunnel shield and load-deflection behavior of the RC tunnel under the static load and fire effect. The authors consider the presented FEM can be improved with future full-scale fire tests and the analytical approaches and can be utilized for parametric studies.

## Contribution of Researchers

Author 1 and Author 2 have together carried out the part of the present research which are the literature review, the determination of the experimental study that exists in the literature for validation of numerical analysis, the development of the proposed finite element model, and the comparison and interpretation of the results obtained from numerical analysis and experiments.

## Conflict of Interest

The authors have declared no conflict of interest.

## References

- ABAQUS, (2014). ABAQUS/Standard user's manual version 6.14, Hibbit, Karlsson, & Sorensen, Inc.
- Alhawat, H., Hamid, R., Baharom, S., Azmi, M. R. & Kaish, A. B. M. A. (2021). Thermal behaviour of unloaded concrete tunnel lining through an innovative large-scale tunnel fire experimental testing setup. *Construction and Building Materials*, 283,122718. doi: 10.1016/j.conbuildmat.2021.122718.
- ASTM, (2015). Standard test methods for fire tests of building construction and materials, West Conshohocken (PA): ASTM E119.
- Birtel, V. & Mark, P. (2006). Parameterised finite element modelling of RC beam shear failure. *Proceedings of the 19th Annual International ABAQUS Users' Conference*, Boston.
- Boxheimer, S., Knitl, J. & Dehn, F. (2009), Fire test on precast tunnel segments for the Liefkenshoekspoortunnel in Antwerp. *Proceedings of 1st International Workshop on Concrete Spalling due to Fire Exposure*, Leipzig.
- Caner, A. & Böncü, A. (2009). Structural Fire Safety of Circular Concrete Railroad Tunnel Linings. *Journal of*

- Structural Engineering*, 135, 9, 1081–1092. doi: 10.1061/(asce)st.1943-541x.0000045.
- CEN (European committee for standardization). Eurocode 1: Actions on structures. EN 1991-1-1:2002.
- CEN (European committee for standardization). Eurocode 2: Design of concrete structures – Part 1-2: General rules – structural fire design. EN1992-1-2; 2004.
- CEN (European committee for standardization), Eurocode 3: Design of steel structures – Part 1-2: General rules – structural fire design. EN1993-1-2; 2005.
- Dai, J.-G., Gao, W.-Y., & Teng, J. G. (2015). Finite Element Modeling of Insulated FRP-Strengthened RC Beams Exposed to Fire. *Journal of Composites for Construction*, 19, 2, 1-15. doi: 10.1061/(ASCE)CC.1943-5614.0000509.
- Gao, W. Y., Dai, J. G., Teng, J. G., & Chen, G. M. (2013). Finite element modeling of reinforced concrete beams exposed to fire. *Engineering Structures*, 52, 488–501. doi:10.1016/j.engstruct.2013.03.017.
- Guerrieri, M., Sanabria, C., Lee, W. M., Pazmino, E. & Patel, R. (2020). Design of the metro tunnel project tunnel linings for fire testing. *Structural Concrete*, April, 1–29. doi: 10.1002/suco.202000140
- Haack, A. (1992). Fire protection in traffic tunnels-initial findings from large-scale tests. *Tunnelling and Underground Space Technology*, 7, 4, 363–375. doi: 10.1016/0886-7798(92)90066-Q.
- Haack, A. (1998). Fire protection in traffic tunnels: General aspects and results of the EUREKA project. *Tunnelling and Underground Space Technology*, 13, 4, 377–381. doi: 10.1016/S0886-7798(98)00080-7.
- Hajiloo, H. & Green, M. F. (2018). GFRP reinforced concrete slabs in fire: Finite element modelling. *Engineering Structures*, 183, October 2018, 1109–1120. doi: 10.1016/j.engstruct.2019.01.028.
- Hua, N., Khorasani, N. E., Tessari, A. & Ranade, R. (2022). Experimental study of fire damage to reinforced concrete tunnel slabs. *Fire Safety Journal*, 127, 103504. doi: 10.1016/j.firesaf.2021.103504.
- Hua, N., Khorasani N. E. & Tessari, A. (2022). Numerical modeling of the fire behavior of reinforced concrete tunnel slabs during heating and cooling. *Engineering Structures*, 258, 114135. doi: 10.1016/j.engstruct.2022.114135.
- International Tunnelling and Underground Space Association (ITA), 2005. Guidelines for structural fire resistance for road tunnels.
- ISO, (1999). Fire resistance tests-Elements of building construction-Part 1: General requirements, Geneva (Switzerland): ISO 834-1.
- Jiang, L., Orabi, M. A., Jiang, J. & Usmani, A. (2021). Modelling concrete slabs subjected to fires using nonlinear layered shell elements and concrete damage-plasticity material. *Engineering Structures*, 234, 111977. doi: 10.1016/j.engstruct.2021.111977.
- Kaundinya, I., Dehn, F., Nause, P. & Juknat, M. (2009). Fire tests at large-scale specimens of ZTV-ING conform fiber-modified concrete for inner shells of road tunnels. *Proceedings of 1st International Workshop on Concrete Spalling due to Fire Exposure*, Leipzig.
- Li, C., Hao, H. & Bi, K. (2017). Numerical study on the seismic performance of precast segmental concrete columns under cyclic loading. *Engineering Structures*. 148, 373–386. doi: 10.1016/j.engstruct.2017.06.062
- Lönnermark A. (2005). *On the characteristics of fires in tunnels* (Doctoral thesis). Lund University, Sweden.
- Mirza, O. & Uy, B. (2009). Behaviour of headed stud shear connectors for composite steel-concrete beams at elevated temperatures. *Journal of Constructional Steel Research*, 65, 662–74. doi: 10.1016/j.jcsr.2008.03.008.
- National Fire Protection Association (NFPA), (1998). NFPA 502 standard for road tunnels, bridges, and other limited access highways, NFPA 502.
- Pagani, R., Bocciarelli, M., Carvelli, V., & Pisani, M. A. (2014). Modelling high temperature effects on bridge slabs reinforced with GFRP rebars. *Engineering Structures*, 81, 318–326, doi: 10.1016/j.engstruct.2014.10.012.
- Richter, E. (2005). Fire test on single-shell tunnel segments made of a new high-performance fireproof concrete. *Workshop: Fire Design of Concrete Structures: What now*.
- Shen, Y., Zhu, H., Yan, Z., Zhou, L. & Lu, Y. (2021). Semi-analytical thermo-mechanical model for the shield tunnel segmental joint subjected to elevated temperatures. *Tunnelling and Underground Space Technology*, 118, 104170. doi: 10.1016/j.tust.2021.104170.
- Siemon, M., & Zehfuß, J. (2018). Behavior of structural tunnel elements exposed to fire and mechanical loading. *Journal of Structural Fire Engineering*, 9, 2, 138–146. doi: 10.1108/JSFE-01-2017-0020.
- Yan, Z. G., Zhu, H. H., Ju, J. W. & Ding, W. Q. (2012). Full-scale fire tests of RC metro shield TBM tunnel linings. *Construction and Building Materials*, 36, 484–494. doi: 10.1016/j.conbuildmat.2012.06.006.

- Yan, Z. G., Shen, Y., Zhu, H. H., Li, X. J., & Lu, Y. (2015). Experimental investigation of reinforced concrete and hybrid fibre reinforced concrete shield tunnel segments subjected to elevated temperature. *Fire Safety Journal*, 71, 86–99, 2015, doi: 10.1016/j.firesaf.2014.11.009.
- Yasuda, F. & Ono, K. (2004). Fire protection for TBM shield tunnel lining. *Tunnelling and Underground Space Technology*, 19, 4–5, 317. doi: 10.1016/j.tust.2004.01.018.
- Yılmaz, T., Kirac, N., Anil, Ö., Erdem, R. T., & Sezer, C. (2018), “Low-velocity impact behaviour of two way RC slab strengthening with CFRP strips,” *Construction and Building Materials*, 186, 1046–1063. doi: 10.1016/j.conbuildmat.2018.08.027.
- Yılmaz, T., Kirac, N., Anil, Ö., Erdem, R. T., & Hoşkal, V. (2020). Experimental and numerical investigation of impact behavior of reinforced concrete slab with different support conditions. *Structural Concrete*, September,1–19. doi: 10.1002/suco.202000216.
- Yılmaz, T., Kirac, N., Anil, Ö., Erdem, R. T., & Kacaran, G. (2020). Experimental Investigation of Impact Behaviour of RC Slab with Different Reinforcement Ratios. *KSCE Journal of Civil Engineering*, 24, 1, 241–254. doi: 10.1007/s12205-020-1168-x.